Journal of Alloys and Compounds 688 (2016) 497–503

Contents lists available at ScienceDirect

Journal of Alloys and Compounds

journal homepage: http://www.elsevier.com/locate/jalcom

Short-range structure and photoluminescent properties of the $CaTiO_3$:Pr,La phosphor

Guilherme K. Ribeiro [a], Fabio S. Vicente [a], Maria Inês B. Bernardi [b], Alexandre Mesquita [a, *]

[a] Instituto de Geociências e Ciências Exatas, UNESP – Univ Estadual Paulista, Departamento de Física, Rio Claro, SP, Brazil
[b] Instituto de Física de São Carlos, Universidade de São Paulo, São Carlos, SP, Brazil

ARTICLE INFO

Article history:
Received 13 April 2016
Received in revised form
5 July 2016
Accepted 7 July 2016
Available online 9 July 2016

Keywords:
$CaTiO_3$
Calcium titanate
Praseodymium
Lanthanum
Photoluminescence
Red phosphor
XANES
Raman
Ca vacancies
Short term afterglow

ABSTRACT

Pr^{3+}-doped $CaTiO_3$ perovskite is a promising phosphor compound with the possibility of use in several technological applications. In this paper, we report the substitution of Ca^{2+} ions with La^{3+} ions in order to promote Ca vacancies to further enhance photoluminescence (PL). $CaTiO_3$:Pr,La samples were prepared by the polymeric precursor method and their short- and long-range structure and photoluminescent properties were investigated in this paper. PL measurements show a narrow emission centered at 612 nm typical of the $^1D_2 - {}^3H_4$ transition of Pr^{3+} ions. As the La content increases, the intensity of this peak is increased. This enhancement of PL curves for $CaTiO_3$:Pr,La samples is associated with disorder in the $CaTiO_3$ lattice caused by the La incorporation. This disorder as a function of the La content is shown by both X-ray absorption near edge structure (XANES) spectra at the Ti K-edge and Raman spectroscopy measurements. $CaTiO_3$:Pr,La samples do not present PL with long term afterglow.

1. Introduction

Luminescent materials, or phosphors, are widely used in several technological applications, such as cathode-ray tubes, light bulbs, lasers, solar concentrators, vacuum fluorescent displays, medical radiology equipment (including scintillators), field emission displays and light-emitting diodes [1–7]. Regarding field emission displays, which are one of the best candidates for advanced flat-panel applications, calcium titanate doped with praseodymium ($CaTiO_3$: Pr^{3+}) is a promising phosphor material for this application [1,3].

Since the publication of results reporting red emission from $CaTiO_3$: Pr^{3+}, the study and development of this material, which aims to find applications such as phosphor, has received much attention [2,8–11]. This red emission at around 612 nm is ascribed to the 4*f*–4*f* transition from the excited state $^1D_2$ to the ground state $^3H_4$ of Pr^{3+} ions. The excitation of the luminescence is achieved through the conduction band states of the orthorhombic $CaTiO_3$ lattice and then transferred to the emitting level [8,9]. Moreover, compared to conventional sulfide compounds, $CaTiO_3$:Pr^{3+} presents better physical and chemical stabilities due to the fact that it is an oxide phosphor [12]. Trivalent praseodymium is well-known to emit efficiently between the blue and the red regions, depending on the host material, the concentration and the pumping conditions [13]. $CaTiO_3$:Pr^{3+} phosphor exhibits red cathodoluminescence with CIE coordinates (chromaticity coordinates) at x = 0:680 and y = 0:311, very close to the coordinates of the "ideal red", which is rather attractive for potential applications [13].

Many efforts have been employed in order to improve optical properties of this material, such as intensity of excitation/emission and phosphorescent decay [9,10,12,14–16]. For this purpose, different methods of synthesis, co-doping, controlling of particle size and annealing have been used [9,10,12,14–17]. Co-doping of $CaTiO_3$:Pr^{3+} with Bi^{3+} greatly enhances UV excitation in the spectral range 370–390 nm [16,18], whereas enhancement of the photoluminescence (PL) intensity of $CaTiO_3$:Pr^{3+} can also be

* Corresponding author. Departamento de Física, Instituto de Geociências e Ciências Exatas, Universidade Estadual Paulista, Rio Claro, SP, Brazil.
E-mail address: mesquita@rc.unesp.br (A. Mesquita).

http://dx.doi.org/10.1016/j.jallcom.2016.07.090
0925-8388/

achieved by adding H_3BO_3 or B_2O_3 as flux [16,19,20]. Substitution of Na^+ or Ag^+ cations for Ca^{2+} and substitution of trivalent cations, like Al^{3+}, or divalent cations, like Mg^{2+} or Zn^{2+} for Ti^{4+} cations, were also used as methods that improved the red emission or afterglow [9,16]. This improvement is attributed to the formation of trapping centers related to the reduction of Pr^{3+} defects due to the charge compensation which increases the energy transfer from $CaTiO_3$ to Pr^{3+} [4,16,19,20]. If there is no other charge compensation, some undesirable defects, such as Ti^{3+} and oxygen vacancies, may form near Pr^{3+}, which can contribute to quench the Pr^{3+} emission [4].

Thus, substitutions of monovalent cations for Ca^{2+} and trivalent cations for Ti^{4+} are used in order to achieve charge compensation. On the other hand, a calcium vacancy can be promoted to achieve charge compensation due to fact that Pr^{3+} is typically thought to occupy a Ca^{2+} site [4]. In this case, the formula $Ca_{1-3x/2}Pr_xTiO_3$ is usually adopted and the charge compensation occurs by $x/2$ formula units of Ca vacancies per formula units of Pr^{3+}. As every Ca vacancy is close to the Pr^{3+} ion in the lattice and Pr^{3+} concentration is quite low, statistically, the possibility of the Ca vacancies meeting the Pr^{3+} ions is not favorable [4]. Regrettably, there are so few reports in the literature concerning this kind of study [4]. Hence, in this paper we report the substitution of Ca^{2+} ions by trivalent La ions in order to promote more Ca vacancies than $x/2$ to compensate the additional positive charge. In principle, the disorder structure caused by Ca vacancies can originate lower symmetry at Pr^{3+} sites, which can mix opposite-parity into 4*f* configurational levels, subsequently increasing the $^1D_2$- $^3H_4$ transition probabilities of Pr^{3+} ions and to get the further enhanced luminescence of Pr^{3+} [21]. Calcium titanate doped by praseodymium and lanthanum ($CaTiO_3$:Pr,La) samples were prepared and structural characteristics were probed by several techniques, which are correlated to PL properties.

2. Experimental

$CaTiO_3$:Pr,La samples with a nominal composition of $Ca_{1-3/2(x+y)}La_xPr_yTiO_3$ were prepared by the polymeric precursor method (details of this method can be found elsewhere [22]) with $x = y = 0.00$ (CT), $x = 0.05$ and $y = 0.00$ (CLT5), $x = 0.10$ and $y = 0.00$ (CLT10), $x = 0.05$ and $y = 0.01$ (CLPT5) and $x = 0.10$ and $y = 0.01$ (CLPT10). This method has proven to be an effective procedure for the preparation of nanostructured samples [3,23]. Calcium nitrate tetrahydrate $Ca(NO_3)_2{\cdot}4H_2O$ (99%, Aldrich), titanium isopropoxide $[Ti(OC_3H_7)_4]$ (98%, Aldrich), praseodymium oxide Pr_2O_3 (99.9% Alfa Aesar), lanthanum nitrate hexahydrate (99%, Aldrich), ethylene glycol, $C_2H_6O_2$ (99.5%, Synth) and citric acid $C_6H_8O_7$ (99.5%, Synth) were used as raw materials. Titanium citrate was formed by titanium isopropoxide dissolution in a citric acid aqueous solution under constant stirring. The citrate solution was stirred at 70 °C to obtain a clear homogeneous solution. Stoichiometric quantities of calcium nitrate tetrahydrate, lanthanum nitrate hexahydrate and praseodymium nitrate (Pr_2O_3 was dissolved with HNO_3 to convert into $Pr(NO_3)_3$) were added to the Ti citrate solution. After the cation homogenization in the solutions, $C_2H_6O_2$ was added to promote a polyesterification reaction. The citric acid/ethylene glycol mass ratio was fixed at 60/40. As the preparation involves the polymeric network formation, the samples were heated at 400 °C for 4 h in order to eliminate the organic precursors. After this heat treatment, $CaTiO_3$:Pr,La samples were annealed at 500, 0.600 and 700 °C for 2 h.

In order to confirm the nominal concentration of synthesized samples, a field emission scanning electron microscope (FE-SEM) Zeiss Sigma with an Oxford system of qualitative and quantitative chemical analysis was used. Energy dispersive spectroscopy (EDS) was performed on prepared samples with the following nominal concentration: $Ca_{0.91}La_{0.05}Pr_{0.01}TiO_3$ (CLPT5) and $Ca_{0.885}La_{0.10}Pr_{0.01}TiO_3$ (CLPT10). The average effective cation concentrations measured with EDS analysis were: 0.887 for Ca, 0.055 for La, 0.011 for Pr and 1.058 for Ti (CLPT5 sample) and 0.846 for Ca, 0.099 for La, 0.012 for Pr and1.043 for Ti (CLPT10 sample). For samples without Pr, the effective cation concentrations are: 0.878 for Ca, 0.049 for La and 1.053 for Ti (CLT5 sample) and 0.857 for Ca, 0.101 for La and 1.041 for Ti (CLT10 sample). These results show that the sample compositions are quite similar to the nominal compositions. The EDS spectrum for the CLPT10 sample is shown in Fig. 1.

The X-ray powder diffraction (XRD) measurements were performed at room temperature on a Rigaku Ultima 4 powder diffractometer with geometry θ-2θ, a rotating anode X-ray source (Cu-K_α radiation, $\lambda = 1.542$ Å) and a scintillation detector. The data were collected with a step size of 0.02° and the count time was 5 s per step. Ti K-edge X-ray absorption spectra (4966 eV) were collected at the LNLS (National Synchrotron Light Laboratory, Brazil) facility using the D04B-XAS1 beamline. The LNLS storage ring was operated at 1.36 GeV and 100–160 mA. The spectra were collected in transmission mode using a Si(111) channel-cut monochromator at room temperature. The sample thicknesses were optimized at each edge by the Multi-Platform Applications for XAFS (MAX) software package Absorbix code [24]. Normalized XANES (X-ray absorption near edge structure) spectra were extracted with the MAX-Cherokee code. The theoretical XANES spectra were calculated by the FEFF9 *ab initio* code [25] whose input files were issued from MAX-Crystalffrev software, which takes into account substitution disorder and random vacancies in the structure [24]. Raman spectra were measured with a MonoVista CRS Raman spectrometer from S&I. The samples were irradiated with a laser beam focused with an Olympus microscope. For the excitation in backscattering geometry, the 633 nm line of a He-Ne laser with 35 mW was used. Photoluminescence spectra were collected with a Thermal Jarrel-Ash Monospec monochromator and a Hamamatsu R446 photomultiplier. The 350.7 nm exciting wavelength of a krypton ion laser (Coherent Innova) was used; the output of the laser was maintained at 200 mW. The phosphorescence decay curve was measured using a Varian Cary Eclipse fluorescence spectrophotometer. All measurements were taken at room temperature.

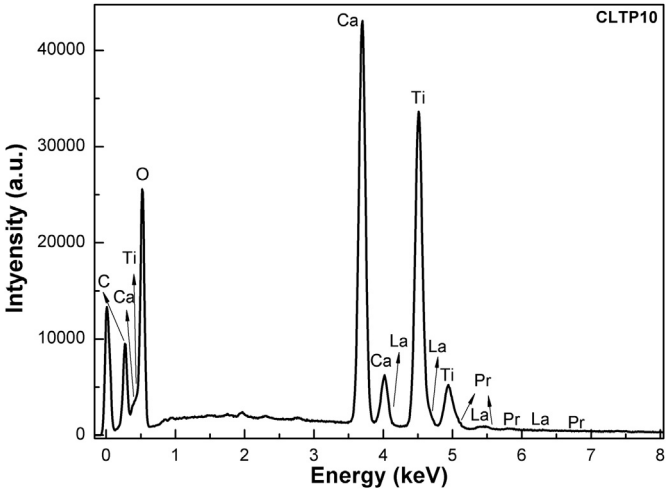

Fig. 1. EDS spectrum for CLPT10 sample annealed at 700 °C.

3. Results and discussion

Fig. 2 shows the X-ray diffraction (XRD) patterns collected at room temperature as a function of the annealing temperature. The samples crystallized completely without the presence of secondary phases and the samples annealed at 500 °C exhibited a pattern characteristic of an amorphous phase. In good agreement with the literature, the diffraction planes of $CaTiO_3$:Pr,La samples annealed at 600 and 700 °C correspond to an orthorhombic structure with *Pbnm* space group [3]. The diffraction planes corresponding to this space group were also indexed in Fig. 2 (JCPDS card N. o 22-0153). Table 1 shows the lattice parameters calculated using least squares fitting for $CaTiO_3$:Pr,La samples annealed at 700 °C. The cell parameters, a, b and c, and the volume of unit cell show a slight increase as a function of La and Pr content. This minor increase is consistent with the presence of cation vacancy which can induce a lattice expansion in order to minimize anion repulsions in the vicinity of the vacancy.

In $CaTiO_3$, Pr^{3+} can substitute for Ca^{2+} because the ionic radius of Pr^{3+} almost coincides with that of Ca^{2+}. The ionic radii of Pr^{3+} in the twelve and six-coordinated state are 1.30 and 0.99 Å, respectively, whereas the ionic radius of Ca^{2+} in twelve-coordinated state is 1.34 Å and the ionic radius of Ti^{4+} in the six-coordinated state is 0.605 Å [4]. Thus, since the samples were prepared considering stoichiometric $Ca_{1-3/2(x+y)}La_xPr_yTiO_3$ formula, Pr^{3+} ions would preferentially occupy Ca sites instead of Ti sites because of the similar ionic radii. Moreover, our X-ray diffraction (XRD) results did not show any secondary phase, suggesting that Pr^{3+} or La^{3+} incorporates into $CaTiO_3$ lattice.

In order to investigate the effect of La and Pr incorporation and annealing temperature on the local order structure around the Ti atom, Ti K-edge XANES spectra were measured. XANES spectra give information on the coordination symmetry and the valence of ions incorporated in a solid. The energy of the absorption edge shifts according to the valence of the absorbing ion, since the binding energy of bound electrons rises as the valence increases. Also, the shape of the absorption edge depends on the unfilled local density of states and the coordination symmetry of the absorbing element. The XANES spectra are shown in Fig. 3(a) and (b).

The pre-edge region of K-edge spectra of some transition metal oxides is characterized by some features several electron volts before the absorption edge [26]. In transition metal oxides that crystallize in centrosymmetric structures, the intensity of these pre-edge features is very small; however, in non-centrosymmetric structures it can be relatively large [26]. According to Vedrinskii et al., the physical origin of the pre-edge feature between 4964 and 4966 eV is related to quadrupolar transitions of t_{2g}-type molecular orbitals located in the absorption atom [26]. The physical origin of the pre-edge feature between 4966 and 4970 eV (shown in more details in the insets of Fig. 3(a) and (b)) is the transition of the

Table 1
Lattice parameters determined by XRD results from$CaTiO_3$:Pr,La samples annealed at 700 °C.

Sample	a (Å)	b (Å)	c (Å)	Volume (Å^3)
CT	5.3966(5)	5.4053(5)	7.6355(5)	222.72(4)
CLT5	5.4079(5)	5.4134(5)	7.6491(5)	223.93(4)
CLTP5	5.4107(5)	5.4196(5)	7.6579(5)	224.56(4)
CLTP5	5.4108(5)	5.4139(5)	7.6518(5)	224.15(4)
CLTP10	5.4129(5)	5.4193(5)	7.6539(5)	224.52(4)

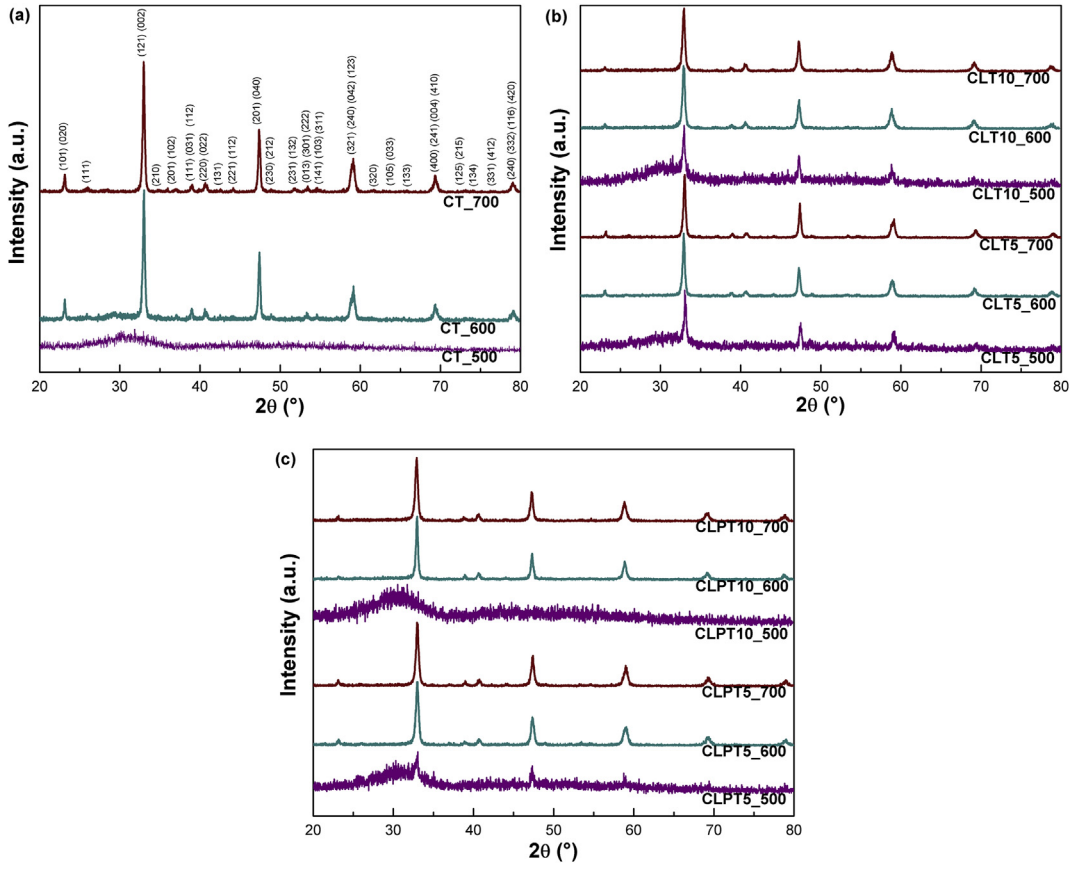

Fig. 2. X-ray diffraction for (a) CT, (b) CLT5 and CLT10, (c) CLPT5 and CLPT10 samples annealed at 500, 600 and 700 °C.

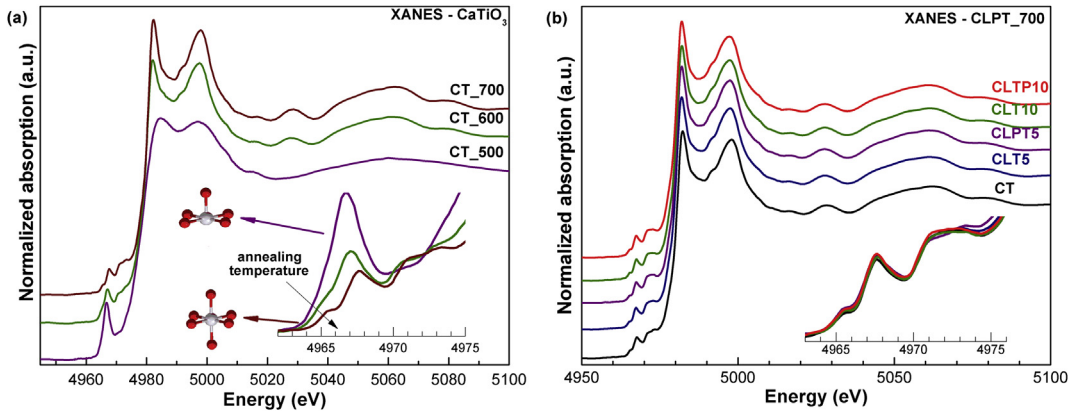

Fig. 3. XANES spectra at the Ti K-edge for (a) CT samples annealed at 500, 600 and 700 °C and (b) for CLT5, CLT10, CLPT5 and CLPT10 samples annealed at 700 °C. The insets magnify the features in the pre-edge region.

metallic 1*s* electron to an unfilled *d* state. This forbidden electronic transition dipole is normally allowed by the mixture of *p* states from surrounding oxygen atoms into the unfilled *d* states of titanium atoms [23,26]. The pre-edge feature between 4970 and 4975 eV in Fig. 3 is related to the Ti 1*s* electron transition to the unoccupied 3*d*-originated e_g-type molecular orbital of TiO_6 polyhedral neighboring the absorbing Ti atoms, which are weakly affected by the core hole potential [26]. The features beyond the absorption edge are related to electronic transitions and the atomic structure of the second and third neighbors of the Ti atom ata distance of up to 8 Å from this atom [27,28].

The XANES spectra for the CT sample as a function of annealing temperature are shown in Fig. 3(a). As the annealing temperature increases, the intensity of all features in pre-edge region decreases. Moreover, the intensity of first features beyond the edge (between 4980 and 5010 eV) increases with the increase of annealing temperature. This behavior is also observed for CLT5, CLT10, CLPT5 and CLPT10 sample (not shown). The higher intensity of these peaks indicates that the local environment of the Ti atom is non-centrosymmetric, which distorts the octahedral configuration [3,23]. This higher intensity has also been attributed to five-fold coordination (TiO_5) clusters [3,23]. In order to confirm this hypothesis, calculated XANES spectra at the Ti K-edge for the $CaTiO_3$ compound using *ab initio* FEFF code [25] were obtained and the results are shown in Fig. 4. The input files for FEFF code, with cluster radius of 6.0 Å, were generated using CRYSTALFFREV software [24] and crystallographic model according to XRD results. As can be seen in Fig. 4, calculated XANES spectra satisfactorily reproduce the experimental spectra. The calculated XANES spectra considering a five-fold coordination of Ti atoms in the $CaTiO_3$ lattice is also shown. The intensity of the pre-edge increases in the XANES spectrum of TiO_5 compared to TiO_6 octahedra, whereas the intensity of features between 4980 and 5010 eV decreases. As stated earlier, the same behavior is observed with decreasing annealing temperature for experimental spectra shown in Fig. 3(a).

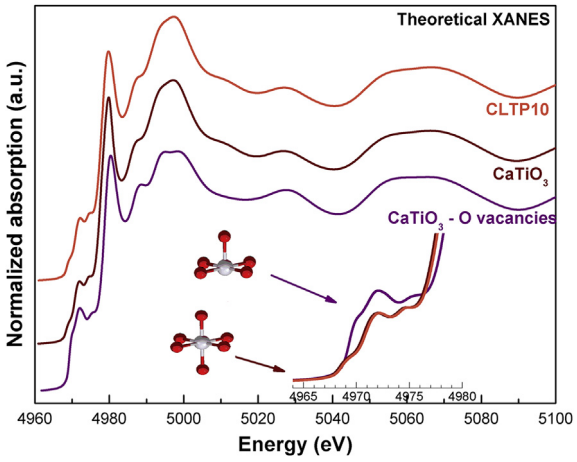

Fig. 4. Calculated XANES spectra for $CaTiO_3$ for five-fold and six-fold Ti coordination and for CLTP10 composition. The inset magnifies the features in pre-edge region.

XANES spectra as a function of La and Pr content for samples annealed at 700 °C are shown in Fig. 3(b). No changes at the pre-edge region are observed as a function of La and Pr concentration. As these transitions are also related to distortion of the octahedral configuration, the incorporation of La^{+3} and Pr^{+3} ions into the $CaTiO_3$ host matrix does not cause structural disorder around the local environmental of Ti atoms. Additionally, O vacancies are not expected, which could also originate from the increasing of the pre-edge features by forming TiO_5 clusters. Moreover, no change in energy was observed for the pre-edge region or the edge for different La and Pr content. This result is corroborated by the calculated XANES for the CLTP10 sample shown in Fig. 3. The *ab initio* calculation was performed considering La atoms and Ca vacancies located in the A-sites of the perovskite lattice stoichiometrically. All transitions in pre-edge and post-edge regions of the experimental spectra were replicated quite well, as can be seen in Fig. 4. No differences in energy or relative intensity of these transitions are observed in calculated the spectrum for the CLTP10 composition compared to that of the CT composition, in agreement with the experimental spectra as a function of the La or Pr content. The displacement of these transitions for lower energies would be an indicative of the decreasing in Ti valence [29]. Therefore, in principle, La and Pr incorporation to the $CaTiO_3$ host matrix does not cause the formation of Ti^{3+} ions according to XANES results.

Raman spectroscopy is a well-known and useful technique for estimating the degree of structural order-disorder at short-range of the materials. Raman spectra of the CT sample annealed at different temperatures are shown in Fig. 5(a). According to literature, there are 24 Raman-active modes for the orthorhombic structure with four molecular units in the primitive cell and space group *Pbnm* ($Z^B = 4$), which can be described by the representation $\Gamma_{Raman,Pbnm} = 7A_g + 5B_{1g} + 7B_{2g} + 5B_{3g}$ [3,30–32]. However, most of these modes cannot be detected because of their low polarizabilities and nine Raman modes (labeled as P_1, P_2, P_3, P_4, P_5, P_6, P_7, P_8 and P_9 in Fig. 4) can be detected in the spectra of the pure CT sample, which are in agreement with previous studies [3,30–32].

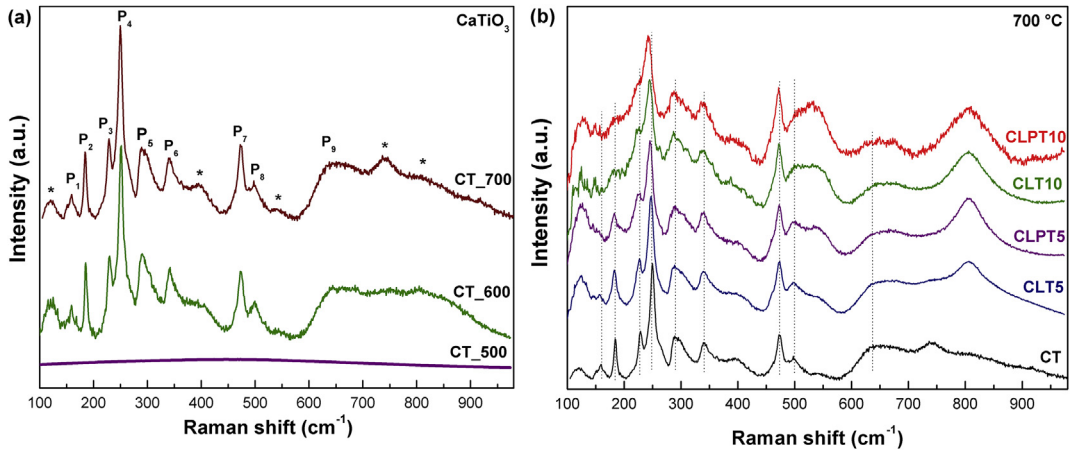

Fig. 5. Raman spectra for (a) CT samples annealed at 500, 600 and 700 °C and (b) CLT5, CLT10, CLPT5 and CLPT10 samples annealed at 700 °C.

Hence, the Raman mode at 160 cm^{-1} is related to the $CaTiO_3$ lattice mode (vibration of Ca bonded to a TiO_3 group (Ca–TiO_3)). Raman modes at 184, 227, 248, 290 and 340 $cm^{-1}$are related to the bending of the O-Ti-O linkages, caused by the "tilt" phenomenon between the TiO_6-α-TiO_6 adjacent clusters (α is the rotation angle between adjacent TiO_6) [30]. The 473 and 499 cm^{-1} Raman modes are ascribed to the Ti-O_6 torsional mode and 636 cm^{-1} Raman mode is assigned to the Ti-O symmetric stretching vibration [3,30–32]. Besides the nine Raman modes, five additional modes, indicated by asterisk in Fig. 5(a), are observed in spectrum for the CT sample. The soft mode at 120 cm^{-1} is not commonly active from first-order Raman scattering in an orthorhombic perovskite-type structure [31]. It is attributed to a perturbation of the perfect crystal symmetry by grain boundaries or second order processes and can be related to the $CaTiO_3$ lattice mode [31]. Additionally, the mode at 539 cm^{-1} can be assigned to Ti-O torsional mode and can also be interpreted as a signal of the disordered structure by an increase in the tilts of the titanium octahedron cluster [31]. The presence of the modes at 393 and 811 cm^{-1} is observed, as well as in other perovskite compounds, and these two modes are characteristic of B-site ordering in complex perovskites [32,33]. The Raman modes at 539 and 811 $cm^{-1}$are related to oxygen motions which can be represented as asymmetric and symmetric "breathing" of the TiO_6 octahedra, respectively [32,33].

In Fig. 5(a), Raman modes are not observed for the CT sample annealed at 500 °C. This result is consistent with XRD results which show an amorphous phase for this sample. As the annealing temperature increases (600 and 700 °C), Raman modes described above are observed, in agreement with XRD results. Raman spectra of $CaTiO_3$:Pr,La annealed at 700 °C are shown in Fig. 5(b). As the La and Pr content increases, the mode labeled P_1 and the mode positioned at 120 cm^{-1} in the CT spectrum shift to lower wavenumbers (intensity of mode at 120 cm^{-1} also increases). Both modes are attributed to the $CaTiO_3$ lattice mode, as stated earlier. An increase of intensity of Raman modes at 539 and 811 cm^{-1} as La^{+3} and Pr^{+3} ions are incorporated to the CT lattice is also observed. These differences in position and intensity is indicative of symmetry break along TiO_6 and CaO_{12} clusters, which is mainly caused by disorder in the lattice modifiers due to distorted CaO_{12} clusters and/or Ca^{2+} vacancies [3,30]. Moreover, no changes are observed in P_2, P_3, P_4, P_5, P_6 and P_9 modes with increasing La and Pr content. As stated earlier, these modes are associated with O-Ti-O bending or Ti-O symmetric stretching. This result is consistent with XANES spectra, which did not show an increase of disorder around Ti atoms with the addition of La and Pr ions.

Fig. 6 depicts the PL curve of $CaTiO_3$:Pr,La samples. PL curves for the CT sample annealed at 500, 600 and 700 °C are shown in Fig. 6(a). A broad peak centered at around 590 nm is observed for the sample annealed at 500 °C, whose structure is amorphous, as shown in the XRD results. As the annealing temperature increases and the CT composition crystallizes, the PL intensity decreases significantly (the inset in Fig. 6 (a) amplifies PL curves for these samples). This behavior was also observed by Lazaro et al. for CT samples; these authors decomposed the PL curve for completed distorted samples in three components that represent different types of electronic transitions which are linked to a specific structural arrangement [23]. Such electronic transitions would be due to the existence of electronic levels in the band gap of a material, which are possible due to structural disorder. These authors propose that PL emission is affected not only by the structural disorder in the network former but also by structural disorder in the network modifier due to charge exchanges between Ca–O_{11} andCa–O_{12} (or TiO_5 and TiO_6) clusters and intermediate levels in the gap state [23]. Our XANES measurements revealed structural disorder as well as the possible presence of TiO_5 for lower annealing temperatures.

Fig. 6(b) shows the PL curves for $CaTiO_3$:Pr,La annealed at 700 °C. The curves for CLT5 and CLT10 samples exhibit a broad peak with low intensity, similar to the CT sample, as expected. On the other hand, CLPT5 and CLPT10 samples reveal a narrow peak centered at 612 nm and its intensity increases as a function of La content. The origin of this peak is well known and ascribed to the 4f–4f transition from the excited state $^1D_2$ to the ground state $^3H_4$ of Pr^{3+} ions [2,8–10]. Some low-intensity peaks are also observed in these PL curves. The features at 705 and 820 nm are related to $^1D_2 - {}^3H_5$ and $^1D_2 - {}^3H_6$ transitions, respectively [34]. The features that are observed in the blue-green region around 500 nm (which are not observed for $CaTiO_3$:Pr compound) could be ascribed to the presence of a La-rich phase, for instance the perovskite $La_{2/3}TiO_3$ [35]. Fig. 6(c) shows the excitation spectrum for 612 nm emission ($^1D_2 - {}^3H_4$ transition) for the CLPT10 sample annealed at 700 °C.

Fig. 7 shows the fluorescence decay time of the emission at 612 nm ($\lambda_{exc} = 350$ nm) for the CLPT10 sample. The decay curve can be well fitted as a function of time by a double exponential equation, in agreement with previous works reporting the fluorescence lifetime of $CaTiO_3$:Pr [12,15]. In Fig. 7, the fit was performed using the following double exponential expression: $I(t) = A_1 e^{t/\tau 1} + A_2 e^{t/\tau 2}$, where I is the fluorescence intensity, A_1 and A_2 are the amplitudes for each component and τ_1 and τ_2 are the decay constants for the two components, respectively [12,15]. The average lifetime for Pr^{3+}

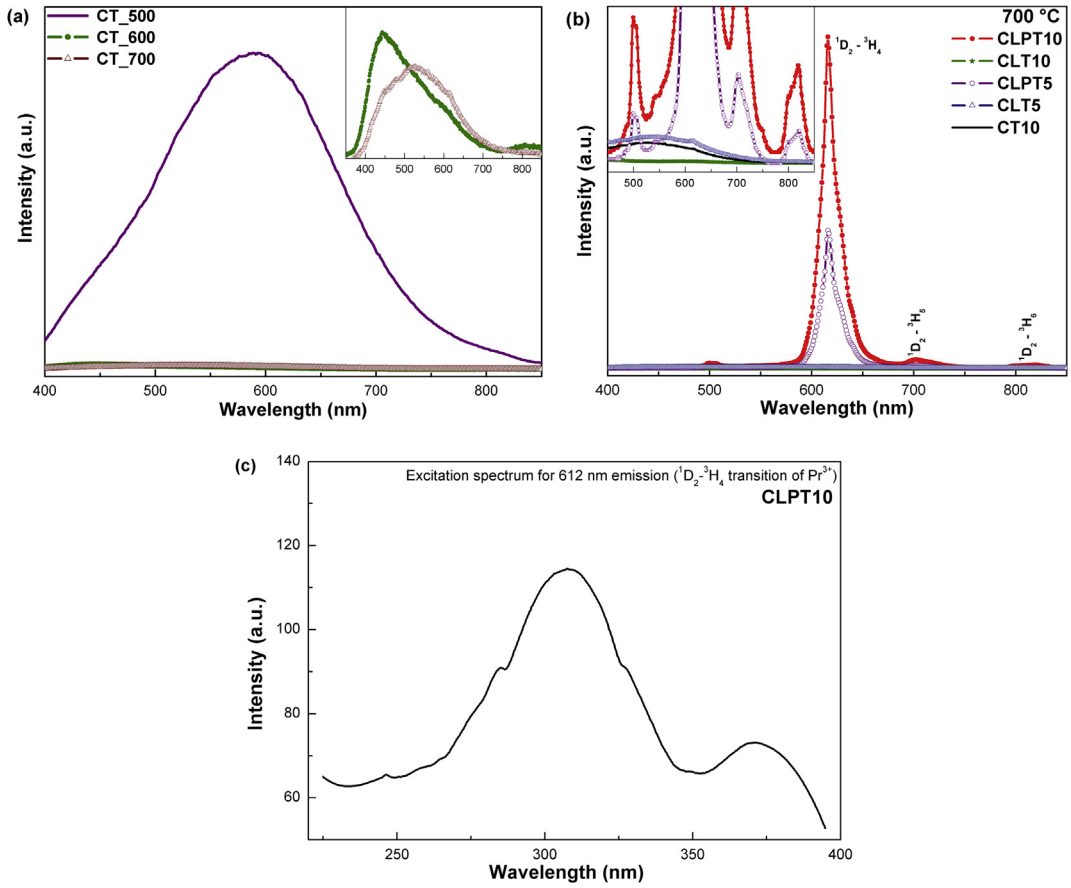

Fig. 6. PL curves for (a) CT samples annealed at 500, 600 and 700 °C, (b) CLT5, CLT10, CLPT5 and CLPT10 samples and (c) the excitation spectrum for 612 nm emission ($^1D_2 - {}^3H_4$ transition) for CLPT10 sample annealed at 700 °C.

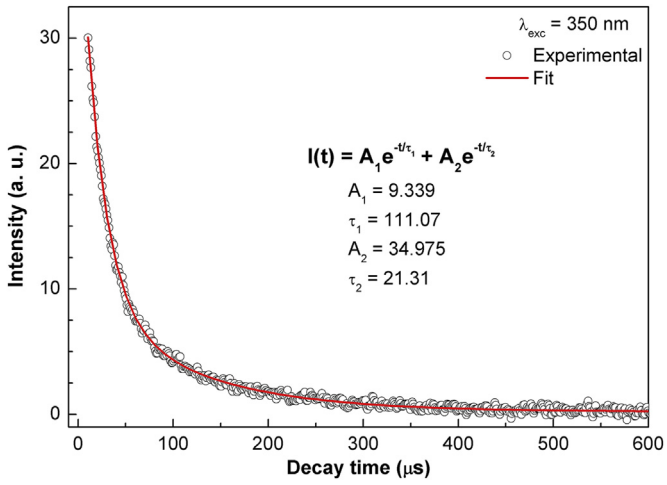

Fig. 7. Fluorescence decay profile for the CLPT10 sample.

can be determined by the formula $\tau = (A_1\tau_1^2 + A_2\tau_2^2)/(A_1\tau_1 + A_2\tau_2)$ [12]. According to the results obtained with the fit, whose values of amplitudes and decay constants are shown in Fig. 7, the average lifetime for the CLPT10 sample is 74 μs It is important to note that the $CaTiO_3$:Pr,La samples do not show PL with long term afterglow. This is an important factor in the synthesis of phosphors for fast response applications [36].

The mechanism of the UV excitation to red emission has been related to energy transfer and charge transfer models of UV photoelectrons to the $^1D_2$ level of Pr^{3+} ions via the valence-to-conduction band transition, Pr^{3+} 4*f*5*d* states, self-trapped excitons and Pr^{4+}/Ti^{3+} states [37]. Several studies have shown an enhancement of red emission from the $CaTiO_3$:Pr host matrix by adding divalent or trivalent cations replacing Ti^{4+}or monovalent cations replacing Ca^{2+} [4,9,16,19,20]. In this case, the formation of trapping centers is related to the reduction of Pr^{3+} defects due to the charge compensation and increases in the energy transfer from $CaTiO_3$ to Pr^{3+}would be associated to this improvement [4,9,16,19,20]. However, in our study, La^{3+} ions are incorporated into Ca^{2+} sites and it is supposed that any additional charge (from La^{+3} or Pr^{3+}) was compensated by the formation of a stoichiometric quantity of Ca vacancies. Therefore, the charge defects are located in the third nearest neighbors of Pr^{3+}. Moreover, distortions can also be located in the 8 s nearest neighbors of Ti^{4+}, as shown by the Raman results. This situation is expected to induce perturbed Pr^{3+} centers that have different optical spectra than those of unperturbed centers, especially concerning the position of $4f^15d^1$bands and charge transfer states [34].

It is well known that the PL efficiency of a rare-earth ion is sensitively influenced by the symmetry and strength of the crystal field and that an increase in the degree of distortion of the crystal field may enhance the rare-earth ion's luminescence efficiency [37]. According to Fujiwara et al., in a study comparing $CaTiO_3$, $SrTiO_3$ and $BaTiO_3$ host lattices, Pr^{3+} substituted for the Ca^{2+} site in $CaTiO_3$:Pr can emit intense red light without the addition of any enhancers, since $CaTiO_3$ has a distorted crystal structure due to the crystal framework constructed by tilted Ti octahedrons [37]. The

ions of large ionic radius or vacancies substituted for A-site ions tend to induce the structure asymmetry of the host, approaching the lower symmetry around Pr^{3+} [21]. In principle, more uneven crystal fields due to the lower symmetry at Pr^{3+} sites can mix opposite-parity into 4*f* configurational levels, subsequently increasing the $^1D_2$- $^3H_4$ transition probabilities of Pr^{3+} ions [21]. As shown by Raman measurements, disorder structure by an augment in the tilts in the titanium octahedron cluster is increased as the La content increases. Thus, the enhancement of the PL curves for $CaTiO_3$:Pr,La samples is associated with disorder in the $CaTiO_3$ lattice caused by La incorporation.

4. Conclusions

$CaTiO_3$:Pr,La samples were prepared by the polymeric precursor method and theirshort- and long-range structures and photoluminescent properties were investigated. PL measurements show a narrow emission centered at 612 nm typical of $^1D_2$-$^3H_4$ transition of Pr^{3+} ions. As the La content increases, the intensity of this peak is increased. This enhancement of PL curves for $CaTiO_3$:Pr,La samples is associated with disorder in the $CaTiO_3$ lattice caused by La incorporation. In principle, more uneven crystal fields due to the lower symmetry at Pr^{3+} sites can mix opposite-parity into 4*f* configurational levels, subsequently increasing the $^1D_2$- $^3H_4$ transition probabilities of Pr^{3+} ions. This disorder, as a function of the La content, was probed by both XANES and Raman measurements.

Acknowledgements

The authors thank FAPESP (through projects 2013/12993-4 and 2013/07909-4) and CNPq funding agencies. The research was partially carried out at LNLS National Laboratory of Synchrotron Light (proposal number XAFS1-17750), Brazil. The authors also thank Prof. Dr. Ervino C. Ziemath and Leandro X. Moreno for Raman measurements and Manoel R. Roncon for EDS measurements.

References

[1] C.S. Lewis, H.Q. Liu, J.Y. Han, L. Wang, S.Y. Yue, N.A. Brennan, S.S. Wong, Probing charge transfer in a novel class of luminescent perovskite-based heterostructures composed of quantum dots bound to RE-activated $CaTiO_3$ phosphors, Nanoscale 8 (2016) 2129–2142.
[2] M. Harada, K. Sakurai, K. Saitoh, S. Kishimoto, Rev. Sci. Instrum. 72 (2011) 4308–4311.
[3] T.M. Mazzo, L.M.R. Oliveira, L.R. Macario, W. Avansi, R.S. André, I.L.V. Rosa, J.A. Varela, E. Longo, Photoluminescence properties of $CaTiO_3$:Eu^{3+} nanophosphor obtained by the polymeric precursor method, Mater. Chem. Phys. 145 (2014) 141–150.
[4] X. Zhang, J. Zhang, X. Zhang, L. Chen, Y. Luo, X. Wang, Enhancement of the red emission in $CaTiO_3$:Pr^{3+} by addition of rare earth oxides, Chem. Phys. Lett. 434 (2007) 237–240.
[5] S. Yoon, E.H. Otal, A.E. Maegli, L. Karvonen, S.K. Matam, S. Riegg, S.G. Ebbinghaus, J.C. Fallas, H. Hagemann, B. Walfort, S. Pokrant, A. Weidenkaff, Improved photoluminescence and afterglow of $CaTiO_3$:Pr^{3+} by ammonia treatment, Opt. Mater. Express 3 (2013) 248–259.
[6] H. Zhong, X.P. Li, R.S. Shen, J.S. Zhang, J.S. Sun, H.Y. Zhong, L.H. Cheng, Y. Tian, B.J. Chen, Spectral and thermal properties of Dy^{3+}-doped $NaGdTiO_4$ phosphors, J. Alloys Compd. 517 (2012) 170–175.
[7] L.L. Noto, S.K.K. Shaat, D. Poelman, M.S. Dhlamini, B.M. Mothudi, H.C. Swart, Cathodoluminescence mapping and thermoluminescence of Pr^{3+} doped in a $CaTiO_3$/$CaGa2O_4$ composite phosphor, Ceram. Int. 42 (2016) 9779–9784.
[8] A. Vecht, D.W. Smith, S.S. Chadha, C.S. Gibbons, J. Vac, Sci. Technol. B 12 (1994) 781.
[9] T. Li, M. Shena, L. Fanga, F. Zhenga, X. Wu, Effect of Ca deficiencies on the photoluminescence of $CaTiO_3$:Pr^{3+}, J. Alloys Comp. 474 (2009) 330–333.
[10] P. Boutinaud, E. Cavalli, R. Mahiou, Photon conversion in Bi_3C/Pr_3C-codoped $CaTiO_3$, J. Phys. Condens. Matter 24 (2012) 295502.
[11] P.T. Diallo, K. Jeanlouis, P. Boutinaud, R. Mahiou, J.C. Cousseins, Improvement of the optical performances of Pr^{3+} in $CaTiO_3$, J. Alloys Compd. 323 (2001) 218–222.
[12] X. Zhang, J. Zhang, X. Ren, X.-J. Wang, The dependence of persistent phosphorescence on annealing temperatures in $CaTiO_3$:Pr^{3+} nanoparticles prepared by a coprecipitation technique, J. Solid State Chem. 181 (2008) 393–398.
[13] P.T. Diallo, P. Boutinaud, R. Mahiou, J.C. Cousseins, Red luminescence in Pr^{3+}-doped calcium titanates, Phys. Status Solidi A 160 (1997) 255–263.
[14] X. Zhang, J. Zhang, X. Zhang, M. Wang, H. Zhao, S. Lu, X.-j. Wang, Size manipulated photoluminescence and phosphorescence in $CaTiO_3$:Pr^{3+} nanoparticles, J. Phys. Chem. C 111 (2007) 18044–18048.
[15] S. Yoon, E.H. Otal, A.E. Maegli, L. Karvonen, S.K. Matam, S.G. Ebbinghaus, B. Walfort, H. Hagemann, S. Pokrant, A. Weidenkaff, Improved persistent luminescence of $CaTiO_3$:Pr by fluorine substitution and thermochemical treatment, J. Alloys Compd. 613 (2014) 338–343.
[16] J. Kaur, V. Dubey, Y. Parganiha, D. Singh, N.S. Suryanarayana, Review of the preparation, characterization, and luminescence properties of Pr^{3+}-doped $CaTiO_3$ phosphors, Res. Chem. Intermed. 41 (2015) 3597–3621.
[17] R.F. Goncalves, A.R.F. Lima, M.J. Godinho, A.P. Moura, J. Espinosa, E. Longo, A.P.A. Marques, Synthesis of Pr^{3+}-doped $CaTiO_3$ using polymeric precursor and microwave-assisted hydrothermal methods: a comparative study, Ceram. Inter 41 (2015) 12841–12848.
[18] M.R. Royce, S. Matsuda, in: United States Patent United States, 1997, pp. 5,656,094.
[19] J. Tang, X. Yu, L. Yang, C. Zhou, X. Peng, Mater. Lett. 60 (2006) 326.
[20] X. Zhang, J. Zhang, X. Zhang, L. Chen, S. Lu, X.J. Wang, J. Lumin. (2007) 958, 122–123.
[21] H.Q. Sun, Q.W. Zhang, X.S. Wang, Y. Zhang, The photoluminescence and electrical properties of lead-free $(Bi_{0.5}Na_{0.5})TiO_3$:Pr ceramics, Ceram. Int. 40 (2014) 15669–15675.
[22] A. Mesquita, M.I. Basso Bernardi, C. Godart, P.S. Pizani, A. Michalowicz, V.R. Mastelaro, Grain size effect on the structural and dielectric properties of $Pb_{0.85}La_{0.15}TiO_3$ ferroelectric ceramic compound, Ceram. Int. 38 (2012) 5879–5887.
[23] S.d. Lazaro, J. Milanez, A.T.d. Figueiredo, V.M. Longo, V.R. Mastelaro, F.S.D. Vicente, A.C. Hernandes, J.A. Varela, E. Longo, Relation between photoluminescence emission and local order-disorder in the $CaTiO_3$ lattice modifier, Appl. Phys. Lett. 90 (2007) 111904.
[24] A. Michalowicz, J. Moscovici, D. Muller-Bouvet, K. Provost, MAX: multiplatform applications for XAFS, J. Phys. Conf. Ser. 190 (2009) 012034.
[25] J.J. Rehr, J.J. Kas, F.D. Vila, M.P. Prange, K. Jorissen, Parameter-free calculations of x-ray spectra with FEFF9, Phys. Chem. Chem. Phys. 12 (2010) 5503–5513.
[26] R.V. Vedrinskii, V.L. Kraizman, A.A. Novakovich, P.V. Demekhin, S.V. Urazhdin, Pre-edge fine structure of the 3d atom K x-ray absorption spectra and quantitative atomic structure determinations for ferroelectric perovskite structure crystals, J. Phys.-Cond. Matter 10 (1998) 9561–9580.
[27] V.R. Mastelaro, A. Mesquita, P.P. Neves, A. Michalowicz, M. Bounif, P.S. Pizani, M.R. Joya, J.A. Eiras, Short-range structure of $Pb_{1-x}Ba_xZr_{0.65}Ti_{0.35}O_3$ ceramic compounds probed by XAS and Raman scattering techniques, J. Appl. Phys. 105 (2009) 033508.
[28] A. Mesquita, A. Michalowicz, V.R. Mastelaro, Local order and electronic structure of $Pb_{1-x}La_xZr_{0.40}Ti_{0.60}O_3$ materials and its relation with ferroelectric properties, J. App. Phys. 111 (2012) 104110.
[29] P. Simon, K. March, O. Stéphan, Y. Leconte, C. Reynaud, N. Herlin-Boime, A.-M. Flank, X-ray absorption investigation of titanium oxynitride nanoparticles obtained from laser pyrolysis, Chem. Phys. 418 (2013) 47–56.
[30] L.H. Oliveira, J. Savioli, A.P.d. Moura, I.C. Nogueira, M.S. Li, E. Longo, J.A. Varela, I.L.V. Rosa, Investigation of structural and optical properties of $CaTiO_3$ powders doped with Mg^{2+} and Eu^{3+} ions, J. Alloys Compd. 647 (2015) 265–275.
[31] G. Huang, W. Dong, L. Fang, F. Zheng, M. Shen, Effects of Eu-doping site on structural and photoluminescent properties of $CaTiO_3$ particles, J. Adv. Dielectr. 1 (2011) 215–221.
[32] H. Zheng, G.D.C.C.d. Györgyfalva, R. Quimby, H. Bagshaw, R. Ubic, I.M. Reaney, J. Yarwood, Raman spectroscopy of B-site order–disorder in $CaTiO_3$-based microwave ceramics, J. Eur. Ceram. Soc. 23 (2003) 2653–2659.
[33] C. Gautam, A.K. Yadav, V.K. Mishra, K. Vikram, Synthesis, IR and Raman spectroscopic studies of (Ba,Sr)TiO_3 Borosilicate Glasses with addition of La_2O_3, Open J. Inorg. Non-metallic Mater 2 (2012) 47–54.
[34] P. Boutinaud, E. Pinel, M. Dubois, A.P. Vink, R. Mahiou, UV-to-red relaxation pathways in CaTiO3:Pr^{3+}, J. Lumin 111 (2005) 69–80.
[35] P. Boutinaud, R. Mahiou, E. Cavalli, M. Bettinelli, Luminescence properties of Pr^{3+} in titanates and vanadates: towards a criterion to predict P-3(0) emission quenching, Chem. Phys. Lett. 418 (2006) 185–188.
[36] L.L. Noto, S.S. Pitale, M.A. Gusowki, J.J. Terblans, O.M. Ntwaeaborwa, H.C. Swart, Afterglow enhancement with In^{3+} codoping in $CaTiO_3$:Pr^{3+} red phosphor, Powder Technol. 237 (2013) 141–146.
[37] R. Fujiwara, H. Sano, M. Shimizu, M. Kuwabara, Quantitative analysis of UV excitation bands for red emissions in Pr^{3+}-doped $CaTiO_3$, $SrTiO_3$ and $BaTiO_3$ phosphors by peak fitting, J. Lumin 129 (2009) 231–237.